Journal of Instrumentation

SISSA

RaDoM2: an improved radon dosimeter

Published by IOP Publishing for Sissa Medialab

Received: *May 20, 2019*
Revised: *August 19, 2019*
Accepted: *September 27, 2019*
Published: *October 16, 2019*

2019 JINST 14 P10019

RaDoM2: an improved radon dosimeter

S. Romano,[b,c,1] **M. Caresana,**[a] **A. Curioni**[b] **and M. Silari**[b]

[a] *Politecnico of Milan, Piazza Leonardo da Vinci 32, Milan, Italy*
[b] *CERN, 1211 Geneva 23, Switzerland*
[c] *UPC, Campus Nord, Calle Jordi Girona, 1-3, Barcelona, Spain*

E-mail: stefano.romano@outlook.com

Abstract: A new dosimeter for radon progeny called RaDoM (Radon Dose Monitor) was recently developed at CERN. RaDoM is an active detector able to directly estimate the effective dose due to the radon progeny. The first version, which used the Timepix hybrid pixel detector, a system of filters and a pump, correctly assessed the effective dose in situations where the environmental conditions are characterized by a standard equilibrium factor, but showed low efficiency for low radon concentrations and in clean air environments. In this improved version, RaDoM2, the Timepix has been replaced by a silicon pin diode. This solution has allowed the optimization of the geometry, the pump flow rate and the associated electronics, improving the performance of RaDoM and substantially reducing its manufacturing costs. This paper describes the RaDoM2, its improved performance compared to RaDoM, the cloud and user interface, tests in a radon chamber and on-the-field measurements.

Keywords: Detector design and construction technologies and materials; Dosimetry concepts and apparatus; Solid state detectors; Spectrometers

[1]Corresponding author.

https://doi.org/10.1088/1748-0221/14/10/P10019

Contents

1 Introduction **1**

2 Material and methods **2**
- 2.1 Silicon diode version 2
- 2.2 Experimental tests 5
- 2.3 Continuous dose measurements 6
- 2.4 Cloud and user interface 9

3 Measurements, results and discussion **10**
- 3.1 Measurement inside the radon chamber 10
- 3.2 Measurements on-the-field and in water reservoirs 11
- 3.3 Discussion 17

4 Conclusions **18**

2019 JINST 14 P10019

1 Introduction

Radon (^{222}Rn), a radioactive noble gas with atomic number 86, is colorless, odorless and tasteless. Radon is the immediate decay product of ^{226}Ra in the ^{238}U series, in turn decaying into a series of short-lived isotopes until stable ^{206}Pb. All radon isotopes are radioactive. Being a noble gas, radon is chemically and electrically inert; after inhalation it is immediately exhaled, and it is therefore only weakly harmful. However, the radon daughter products attach to the ambient aerosol, which may be inhaled and stick to the lung surface. The polonium isotopes, in particular, are alpha emitters that deposit large amounts of energy locally to cells and eventually lead to lung cancer. The major health concern comes from the deposition of radon progeny on the epithelial cells of the bronchial airways. Radon daughters are the largest contributor to daily exposure to radiation. Currently the absorbed dose to lung due to radon exposure is estimated by measuring radon and/or radon progeny concentrations. Due to the recoil energy of the emitted alpha particles, radon decay products are positive ions and attach to ambient aerosol as mentioned above. Furthermore, several building materials attract the particulate, modifying the radioactive equilibrium between radon and its progeny. Other factors, such as humidity, particle size and air exchanges, may also change the radioactive equilibrium. In estimating the dose, default values are assumed for several parameters such as aerosol size, equilibrium factor, particle density and shape, etc, leading to significant uncertainties. A prototype of a new dosimeter for radon progeny called RaDoM (Radon Dose Monitor) [1] was recently developed at CERN. The dosimeter is an active monitor, which directly estimates the effective dose by measuring the energy of alpha particles from the radon progeny, overcoming the need to know the equilibrium factor between radon and its progeny. RaDoM was made of a Timepix detector [2, 3], which is a highly pixelated hybrid silicon sensor, a system of

filters, which simulates the energy deposition in the respiratory track [4], and a small pump for air sampling. RaDoM operated correctly but had low sensitivity, mostly because the geometrical efficiency was limited by the shape of the Timepix board, whereas the power of the air pump was constrained by the fragile wire bonding of the Timepix sensor, which may be broken by a strong air flow. This paper discusses a redesign of the dosimeter that entails the replacement of Timepix by a single, simpler and much cheaper silicon diode. This has allowed optimizing the geometry of RaDoM and increasing the pump flow rate, increasing the detector performance, reducing its manufacturing cost and building a stand-alone device by integrating a microcontroller, overcoming the need of a computer connected to the detector. The new detector, called RaDoM2, uses the same operating principle of RaDoM: the pump draws the air and the radon decay products through the filter, whereas the silicon pin diode counts and measures the energy of alpha particles from the radon daughters, which had attached to the filter. The results of tests in a radon chamber and of extensive measurements in operational conditions are presented

2 Material and methods

2.1 Silicon diode version

The structure of RaDoM2 is shown in figure 1. The 3D model was designed with AUTODESK Inventor [6] and thereafter the detector was 3D printed with a Formlabs Form1 [5], which uses the Stereolithographic (SLA) technology for high precision. The chosen paper filter is the Millipore AA 0.8 µm for its high collection efficiency for radon progeny (99.99 %) [7]. The pump is the NMP830 KNDC model produced by KNF, Germany, with a maximum air sampling rate of 3.1 l/min. The pump is connected to the detector though the central hole on the upper side of the detector. Figure 1 shows the 3D model of the sensor holder. The clips tighten the various parts of the RaDoM2 together. The filter drawer keeps the Millipore filter exactly aligned to the silicon diode at a distance of 6 mm. It is possible to change the filter without disassembling the detector. The apertures on the sides of the detector are for the additional mesh screens, which simulate the absorption characteristics of the lung for the particulate. The geometry of RaDoM2 was imported into the Comsol Multiphysics software [8]. The Comsol Multiphysics modules used for the simulation were CFD, AC/DC and Particle Tracing. The CFD Module is a numerical simulation platform for computational fluid dynamics (CFD) that accurately describes the fluid flow processes, while the AC/DC module is used for simulating electric, magnetic and electromagnetic fields in static and low-frequency applications. The Particle Tracing Module extends the functionality of the Comsol environment for computing the trajectory of particles in a fluid or in a electromagnetic field, including particle-particle, fluid-particle and particle-field interactions. The simulation parameters are listed in table 1. Figure 2 compares the particle trajectories in RaDoM and in RaDoM2. The figures clearly show that in RaDoM the particles disperse close to the sensor area, due to the non-optimized geometry and the lower pump flow rate, leading to a lower collection efficiency, as shown in figure 3. The collection efficiency is defined as the probability that a particle which enters the detector reaches and sticks to the filter. The collection efficiency in RaDoM2 is 26% higher. The time zero is the time when the particle enters the detector. The response of RaDoM2 is faster because the detector is smaller and the particles reach the filter quickly. The chosen silicon diode in RaDoM2 is the Hamamatsu s3204 windowless with an active area of 3.24 cm^2, operated at a bias voltage of 12 V.

2019 JINST 14 P10019

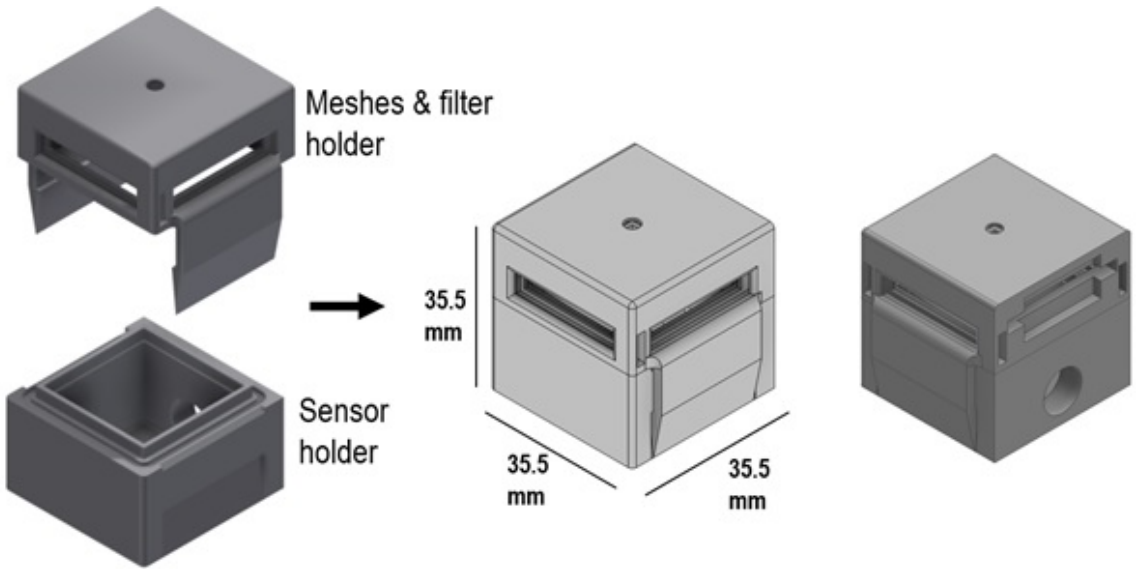

Figure 1. 3D model of the RaDoM2 sensor probe.

Table 1. Simulation parameters.

Forces	**Fluid (air)**	**Particle characteristics**	**Particle release profile**
Pump drag force	Laminar flow	Spherical	3000 samples
Gravity force	293 K temperature	2300 kg/m^3 dust density	Equally distributed from the inlets
Brownian force	Sea level atmospheric pressure	100 nm particle diameter	Initial velocity 0 m/s
Electric force due to the bias voltage of the silicon diode (static field)		Charge particle numbers: 1, 0, -1 equally distributed	
Particles-fluid (air) interaction			
Particles-walls interaction			
Pump drag force			

2019 JINST 14 P10019

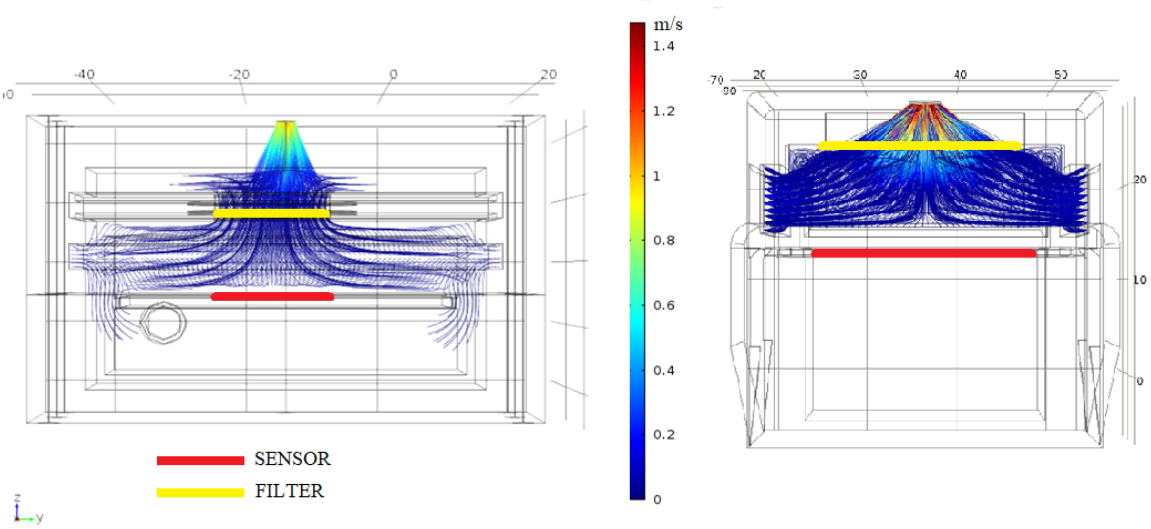

Figure 2. Particle tracing simulations. Left: RaDoM using Timepix. Right: RaDoM 2 using the Si PIN photodiode. Velocity expressed in m/s (color scale).

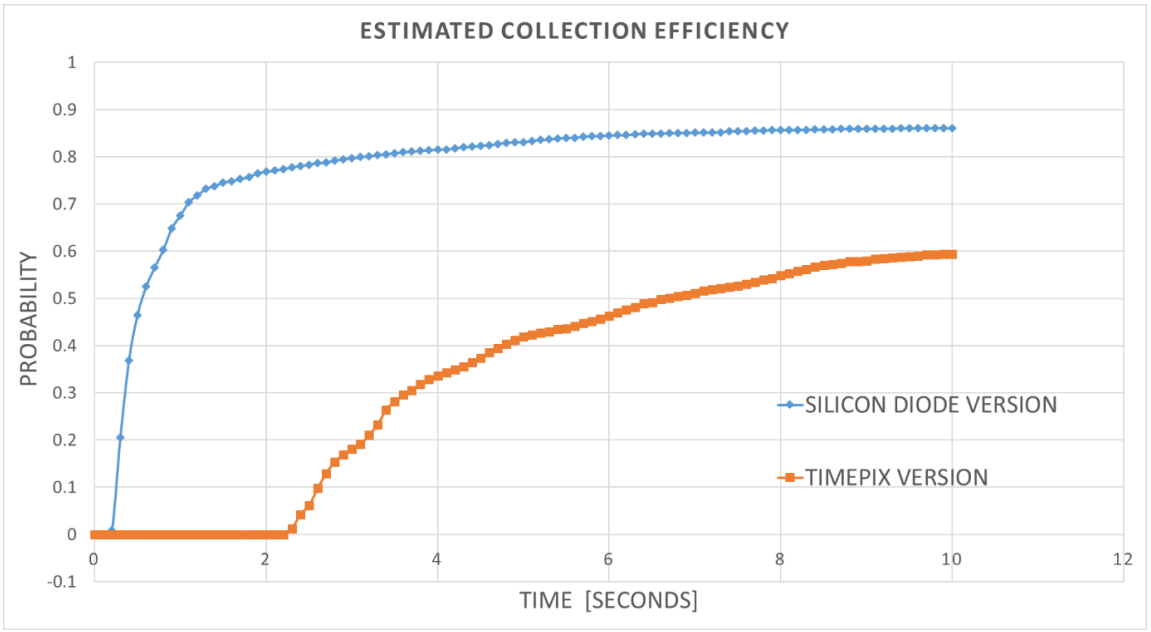

Figure 3. Estimated collection efficiency versus time. Orange: RaDoM. Blue: RaDoM 2.

The diode is connected to a CR-111 [9] charge sensitive preamplifier and a CR-200 [10] Gaussian-shaping amplifier produced by Cremat Inc. Figure 4 shows the block diagram of RaDoM2. The electronic board allows connecting an ionization chamber (RD200M produced by FTLAB [11]) acting as continuous radon monitor. The ion chamber, working in pulse mode, measures the radon concentration whereas the silicon diode measures the radon daughters and estimates the effective dose; the two measurements combined allow estimating the equilibrium factor. The 3D model of the final version of RaDoM2 and a photo of the assembled detector are shown in figure 5.

2019 JINST 14 P10019

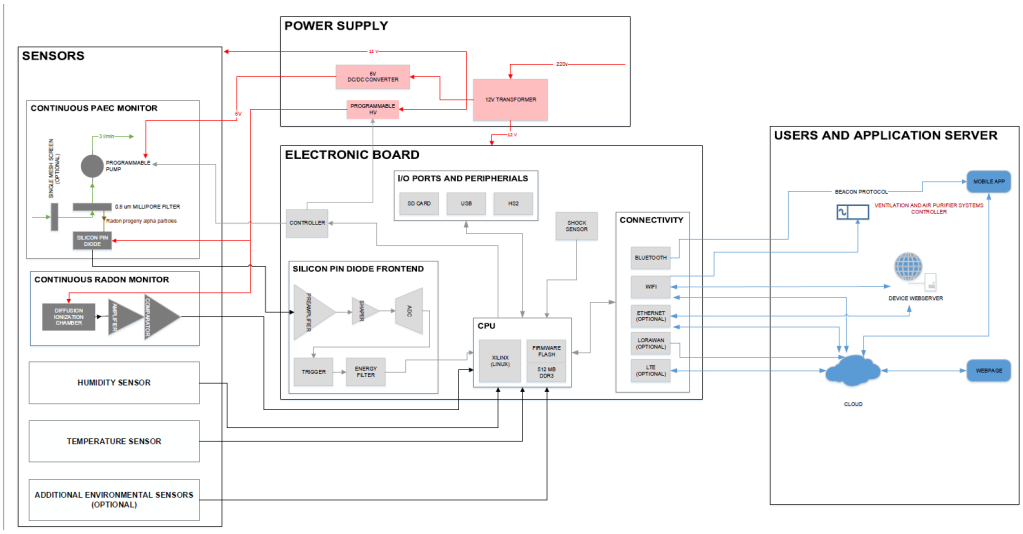

Figure 4. Block diagram of RaDoM2.

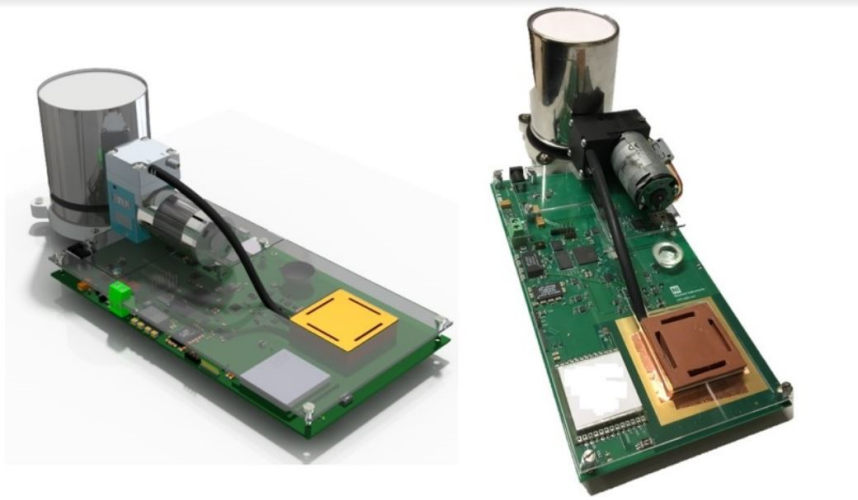

Figure 5. 3D model of the final version of RaDoM2 (left) and the assembled detector (right).

2.2 Experimental tests

Figures 6 and 7 summarize the first test of the device. The test was done with a ^{241}Am source placed on the silicon surface in order to obtain a first energy calibration point. The 4.8 MeV alpha particles reaching the detector generate a signal 115 mV high and 11.5 µs long (figure 6). The energy of the alpha particles impinging on the detector surface is lower than the nominal 5.4 MeV of ^{241}Am due to the source window. The energy distribution of the alpha particles (figure 7) shows a low energy tail, due to the air gap between the source surface and the diode, the source window and to particles incident non-perpendicularly on the silicon diode, inducing an energy degradation. A second test was performed inside the built-in-house radon chamber of CERN Radiation Protection group. The chamber is a box made of acrylic glass with 80 cm × 60 cm × 60 cm dimension (length × width × height) and 0.288 m^3 volume. Radon is normally generated inside the chamber by a ^{226}Ra source,

2019 JINST 14 P10019

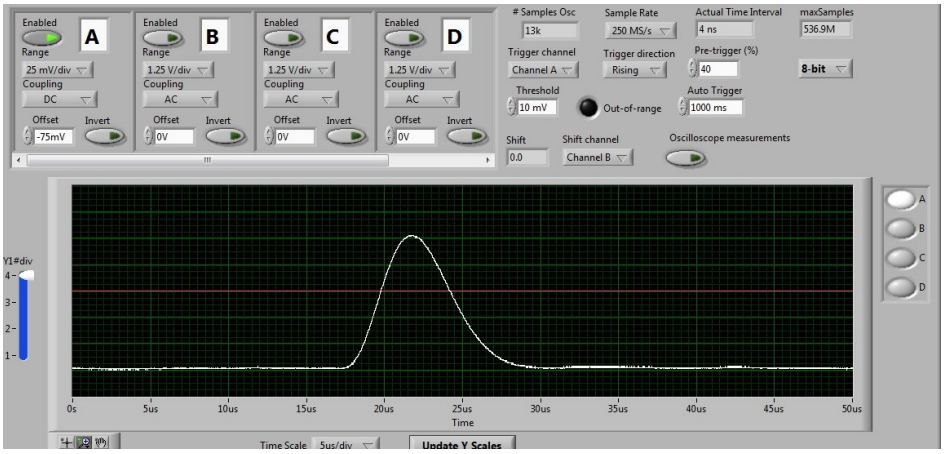

Figure 6. Output signal of the amplifier. Alpha particles from an ^{241}Am source.

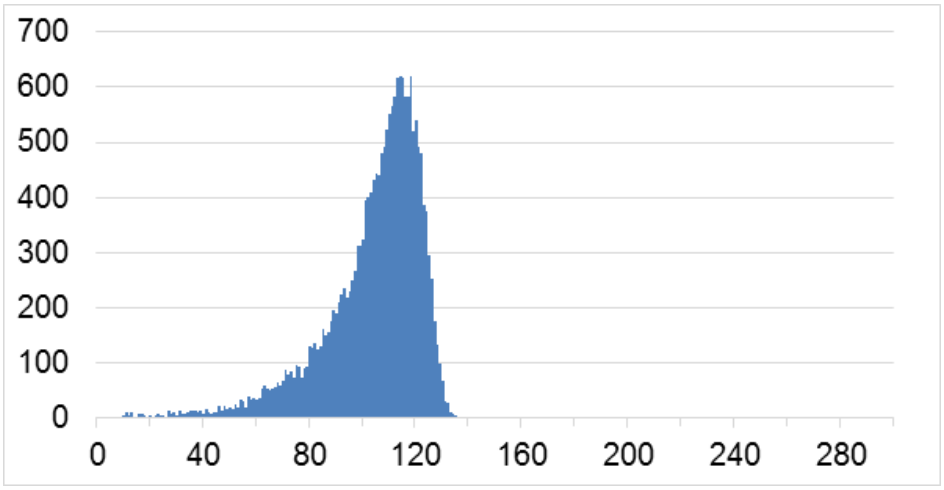

Figure 7. Energy distribution of alpha particles from an ^{241}Am source. Counts versus MCA channel number.

but for this specific test a mixture of sand imported from Brazil was instead used, able to generate significant radon and thoron concentrations. Figure 8 shows the energy distribution of the alpha particles from the radon and thoron progeny. The first peak on the left is the 6 MeV (215 mV) of ^{212}Bi and ^{218}Po, the middle peak is ^{214}Po at 7.7 MeV (278 mV), the peak on the right is ^{216}Po at 8.7 MeV (320 mV). The slight offset (about 2%) is due to the energy resolution of the sensor.

2.3 Continuous dose measurements

The spectrometrc capabilities of RaDoM2 allows discriminating the alpha particles from the ^{218}Po and ^{214}Po isotopes attached to the Millipore filter, but ^{214}Pb and ^{214}Bi cannot be detected, as they are beta emitters. The Potential Alpha Energy Concentration (PAEC) is given by equation (2.1),

$$PAEC = \sum_{1} c_i \frac{PAE_i}{\lambda_i} \tag{2.1}$$

2019 JINST 14 P10019

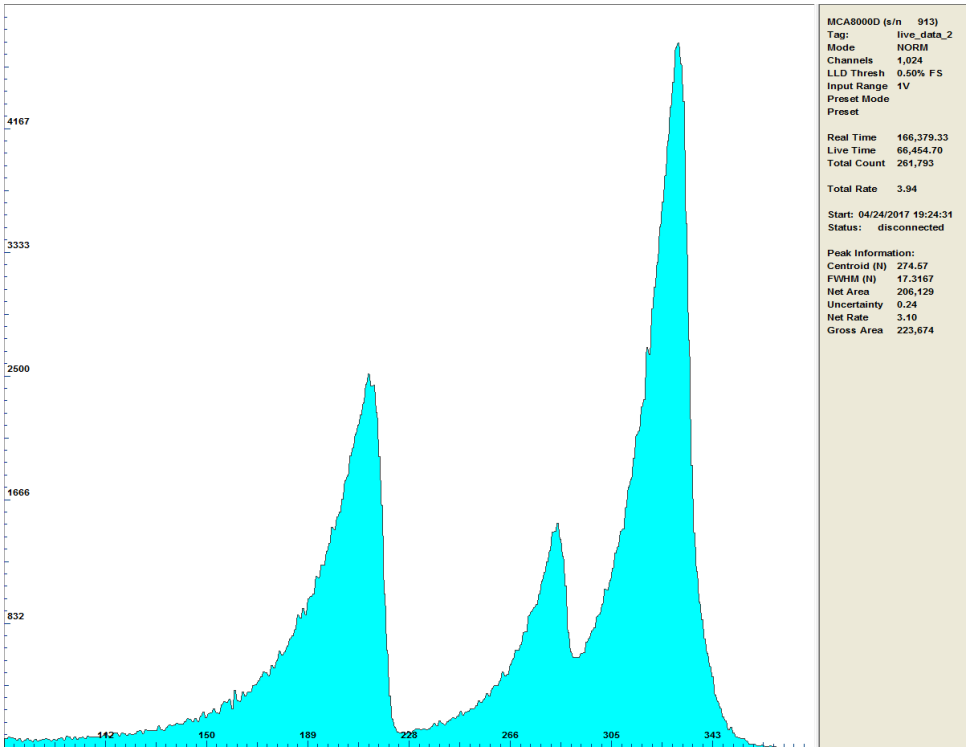

Figure 8. Energy distribution of the alpha particles from the radon and thoron progeny.

where PAE_i is the potential alpha energy of the short-lived radon decay product i, equal to 13.69 MeV for ^{218}Po, and 7.69 for ^{214}Pb and ^{214}Bi, and c_i is the activity concentration of the decay product nuclide i. Since the concentration of the beta emitters is unknown, it is impossible to calculate the potential alpha energy concentration through expression (2.1) [12] without a specific routine. The routine exploits the different half-lives of the radon daughters and a series of counting windows and waiting times. Nevertheless, this routine is not the best method for RaDoM2, because, being a continuous monitor, the pump is always on, and the detector counts the alpha particles during the sampling time window. The method used with RaDoM2 is the following: an air sample is collected on the filter and counted continuously at a flow rate of 3 litres per minute. The total counts are usually calculated for 15 minute intervals. The method is very sensitive since all the collected activity is counted. Furthermore, large air volumes are sampled (approximately 180 liters per hour). One disadvantage of the method is that it calculates the average energy concentration and does not respond quickly: there is a 3 hour response time due to the half-lives of the short lived radon daughters attached to the filter. This means that the actual and the measured energy concentrations may not correspond at a given moment, especially if there are fast changes in environmental conditions. The algorithm is explained in figure 9 and expression (2.2):

$$EC = c1 \cdot c2 \cdot \frac{6 \cdot roi1 + 7.69 \cdot roi2}{e1 \cdot e2 \cdot t \cdot V} \tag{2.2}$$

2019 JINST 14 P10019

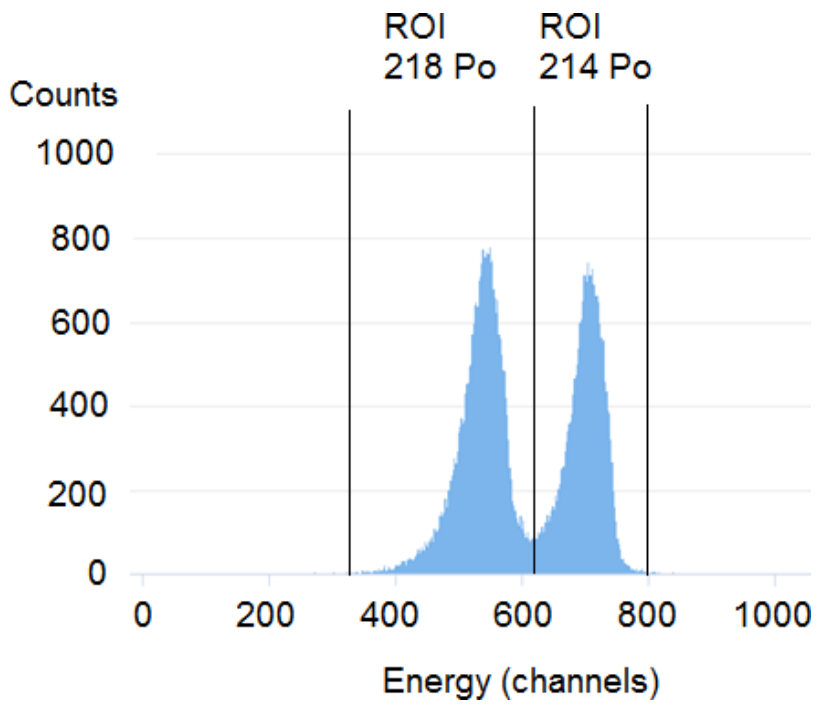

Figure 9. Energy distribution of the alpha particles from radon progeny and regions of interest (ROI).

where:

- EC is the energy concentration expressed in MeV h/m^3.
- $c1$ is a conversion factor: number of samplings per hour, equal to 4, considering a sampling time of 15 minutes.
- $c2$ is a conversion factor: number of litres of air in one cubic meter.
- $roi1$ are the counts in the ^{218}Po ROI (region of interest) during the sampling time.
- $roi2$ are the counts in the ^{214}Po ROI during the sampling time.
- $e1$ is the geometrical efficiency of the detector, equal to 0.4, which is the solid angle subtended by the filter divided by 4π.
- $e2$ is the collection efficiency of the detector, equal to 0.86, estimated by particle tracing simulations (figure 3).
- t is the sampling time, equal to the counting time.
- V is the pump flow rate.

In order to estimate the effective dose, the dose conversion factor proposed by ICRP 137 of 3 mSv per mJ h/m^3 [13] is used.

2019 JINST 14 P10019

2.4 Cloud and user interface

The Linux PC embedded in the board runs a local web server with the graphical interface. Data are sent each 15 minutes to an online server (cloud), accessible from anywhere and from any device connected to the internet. The cloud software, developed in collaboration with the company Nextome S.r.l. (Conversano, Italy) [14], collects raw data from the sensor network and sends them to the Web Engine via https using authentication protocols. The database management system is designed to be flexible and highly scalable, in order to be ready to scale with new data types and higher volumes of data. The system also supports different data types, and offers the possibility to manage users, user groups and users associated to the resources. The row data are analysed directly by the web engine and shown as time series, for both the radon concentration and the effective dose. It is possible to download the data in CVS format and visualize the energy spectra of the radon progeny. Data from the devices can be shown on a map thanks to geolocalization when implemented in the sensor firmware. Figures 10 and 11 show the dashboard of the cloud web-page, showing the status of the installed sensors, the last measured values (their position on the map is not yet implemented), and the data from one detector, respectively.

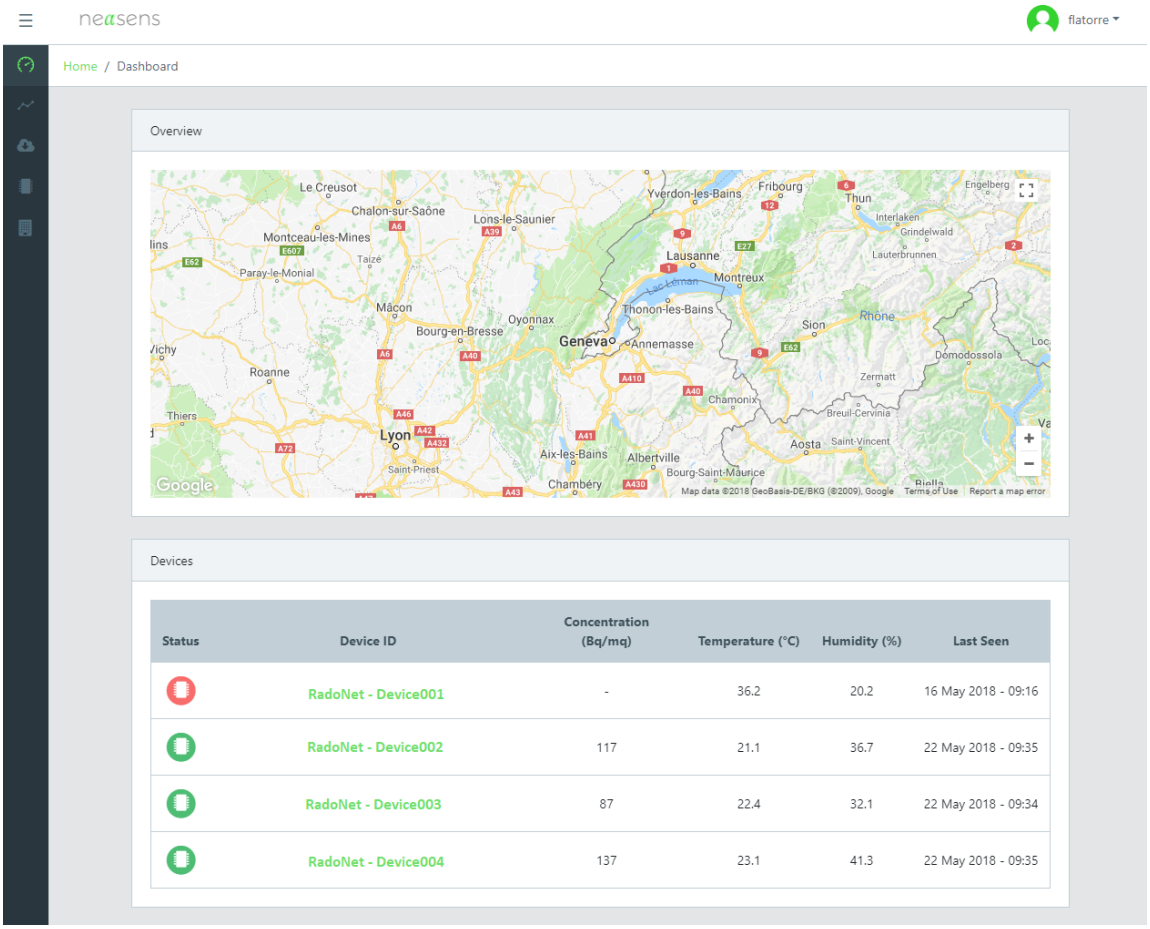

Figure 10. Dashboard view of the web server showing four sensors currently installed in two buildings. The geolocalization is not yet implemented in the sensors firmware, therefore their position is currently not shown on the map.

2019 JINST 14 P10019

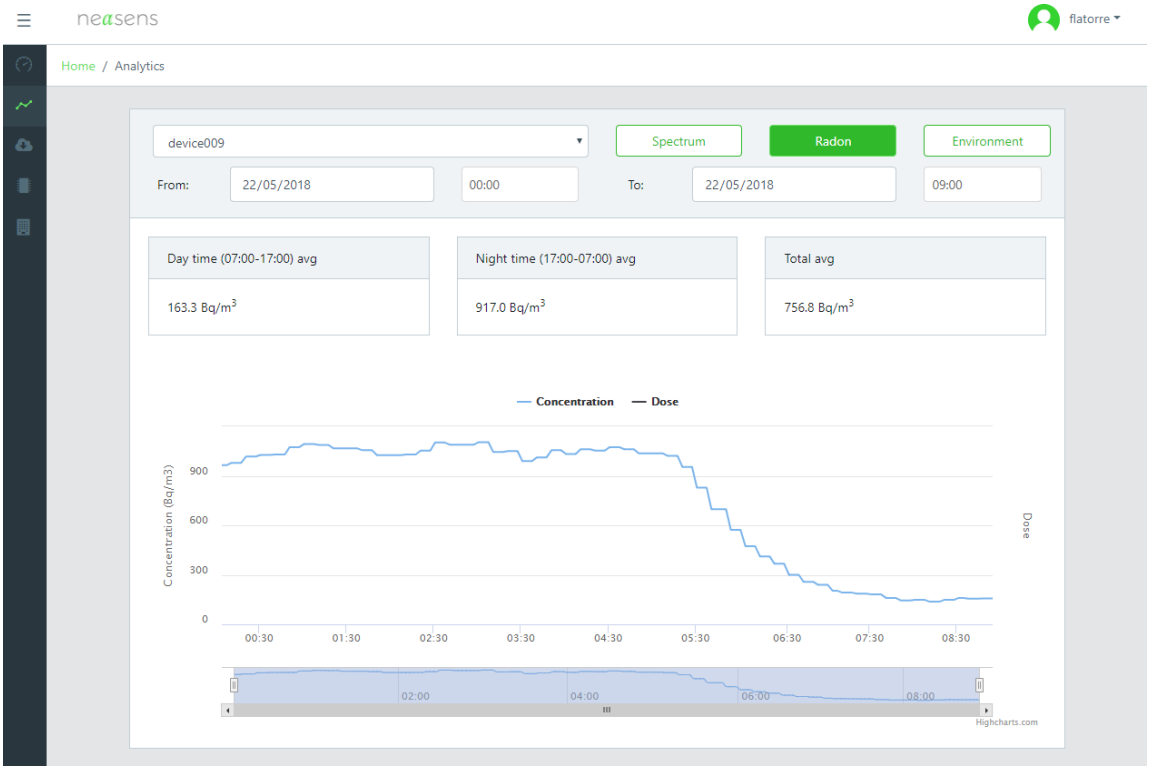

Figure 11. Time series analysis of the radon concentration from RaDoM2 installed in a building.

3 Measurements, results and discussion

3.1 Measurement inside the radon chamber

Under the controlled environmental conditions inside the radon chamber, the effective dose to the lung is generally lower than in a real environment although the radon concentration is typically much higher. This is caused by two phenomena. First, the value of the equilibrium factor is much lower than 0.4 (value usually adopted for dwellings) due to the small volume of the radon chamber used at CERN (0.288 m^3). In fact, the ions of the radon progeny tend to stick to the walls of the chamber rather than lingering in the air. Second, the air inside the chamber is filtered, so it is clean and dust-free. For these reasons, the CERN radon chamber without a particulate generator is not the ideal place to test RaDoM2, but it is nonetheless useful for understanding the behaviour of the detector for very low concentrations of airborne particles and radon daughters. For this purpose, a 22 hour measurement in the radon chamber together with the Radonmapper [15], a professional commercial instrument for monitoring the radon concentration, was performed. Figure 12 shows the integral energy deposition of alpha particles on the RaDoM2 filter. The ^{218}Po and ^{214}Po peaks are evident, whereas the tail on the left side of the histogram is due to counts of stray alpha particles from radon gas. Figure 13 shows the radon concentration measured by the Radonmapper and the effective dose rate inside the radon chamber obtained by RaDoM2. Although the general trend of the effective dose rate follows that of the concentration, the value is much lower than that obtained with on-the-field measurements (see section 3.2) because of the specific environmental conditions

2019 JINST 14 P10019

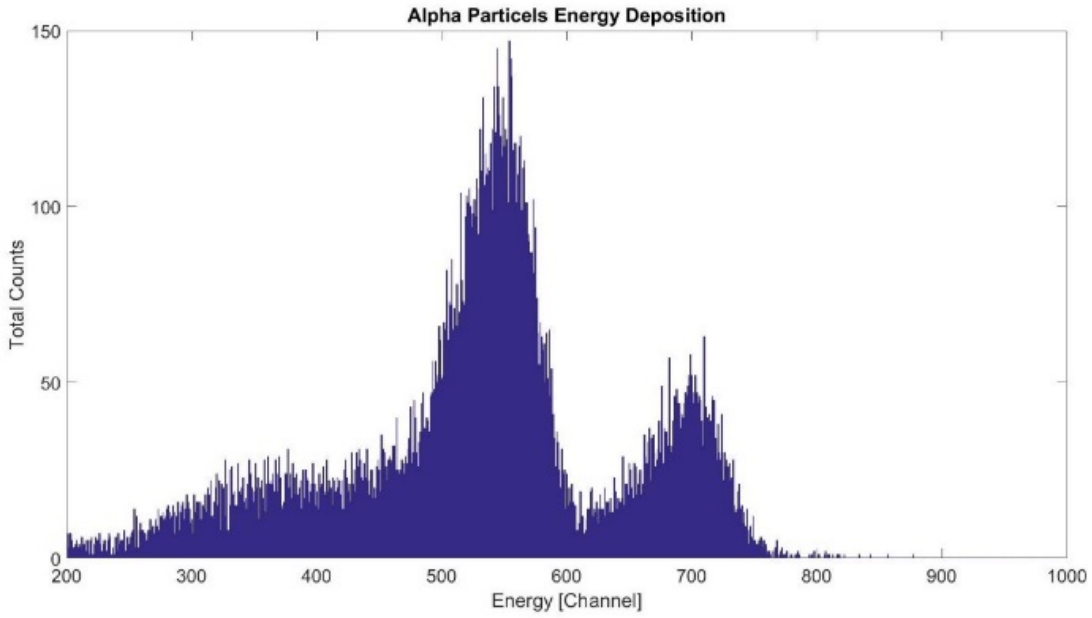

Figure 12. Energy distribution of the alpha particles from radon progeny inside the radon chamber.

inside the chamber as explained above. From the plot the increase of the radon concentration during the first hours (pumping of the radon inside the chamber) is evident, followed by the natural decrease due to the radioactive decay. The disequilibrium between radon and its progeny inside the radon chamber is obvious when plotting the time distribution of the equilibrium factor over the 22 hours of the measurement (figure 14). The average equilibrium factor during this measurement is $(6.6\pm0.5)\cdot10^{-3}$, approximately 60 times lower than the standard indoor value (0.4).

3.2 Measurements on-the-field and in water reservoirs

The radon gas can dissolve and accumulate in groundwater. Water acts as a radon carrier as radon has a high probability to escape from the water into air. If the spring is located indoor, like in spas or water reservoirs, the airborne radon can reach rather high concentration. This section provides a summary of the measurements performed in two water reservoirs in Grenchen, Switzerland, that we will call Grenchen 1 and Grenchen 2. The RaDoM2 was placed in the technical room in Grenchen 1, close to the entrance of the water tank, for 22.5 hours together with a passive CR39 dosimeter, which was left in place for seven days. The average radon concentration measured by the CR39 is 10247±1049 Bq/m^3. For this measurement the ionization chamber integrated in RaDoM2 was not used, since its measuring range is limited to 3700 Bq/m^3. Figure 15 shows the energy deposition in the Millipore mixed cellulose filter by alpha particles from the radon progeny. The peaks due to ^{218}Po and ^{214}Po are evident. A slight hump in both energy peaks can be noticed, which is caused by the unstable current drawn by the pump leading to a baseline signal shift. This problem however only affects the energy resolution and not the integral number of counts. Figure 16 shows alpha energy distribution and the effective dose rate as a function of time. The average effective dose rate estimated by RaDoM2 is in the range 60–110 μSv/h. Considering the average radon concentration measured by the CR39, it is possible to calculate an average radon equilibrium factor of 0.51±0.08.

2019 JINST 14 P10019

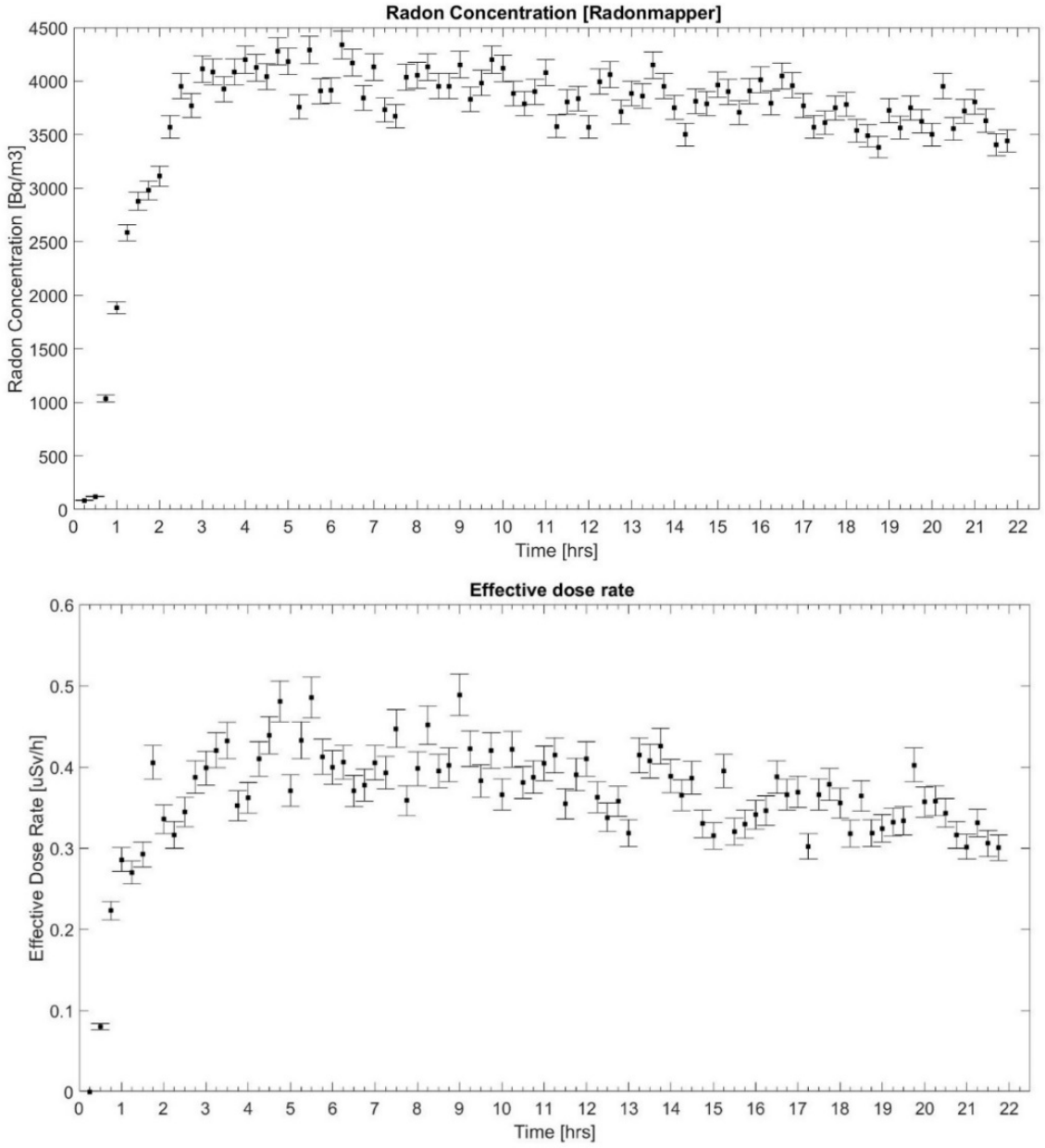

Figure 13. Radon concentration measured by the Radonmapper and effective dose rate inside the radon chamber obtained by the RaDoM2.

Grenchen 2 is a larger water reservoir where school workshops also take place, located a few kilometres from Grenchen 1. The RaDoM2 was placed in the technical room a few meters from the student desks. The measurement lasted 8.7 days; here the radon concentration was measured by the ionization chamber integrated in RaDoM2, since the average concentration was lower than its upper limit of 3700 Bq/m^3. Moreover the average radon concentration could have been lower than the detection limit of 50kBq h/Bq/m^3 of CR39 [16]. The energy deposition by alpha particles from the radon daughters is shown in figure 17. Figure 18 shows the equilibrium factor between

2019 JINST 14 P10019

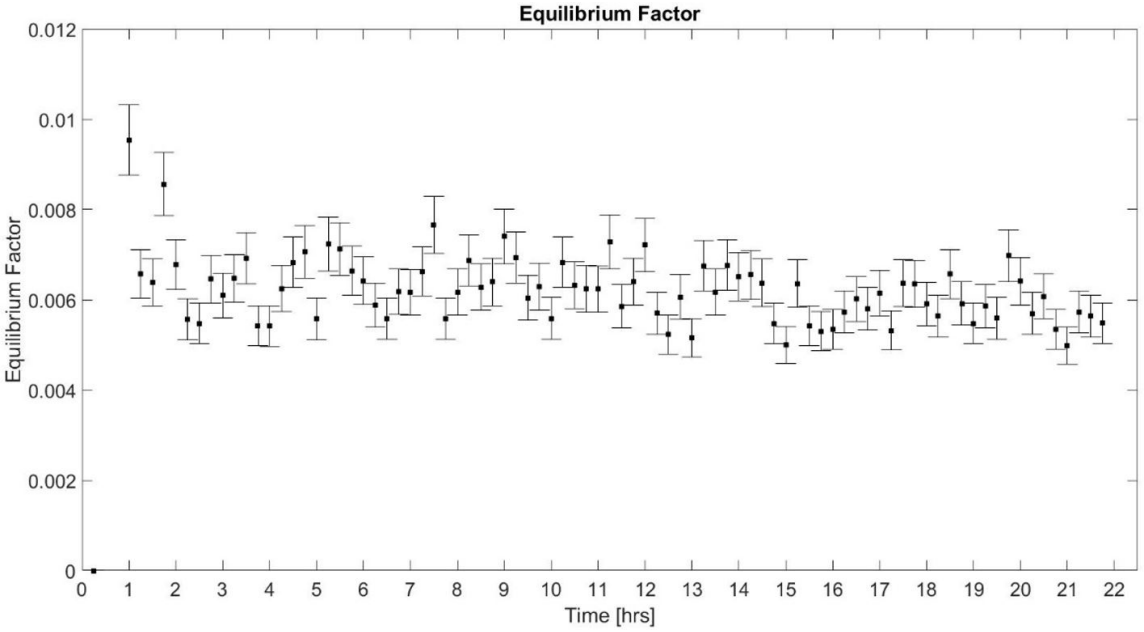

Figure 14. Time variation of the equilibrium factor inside the radon chamber.

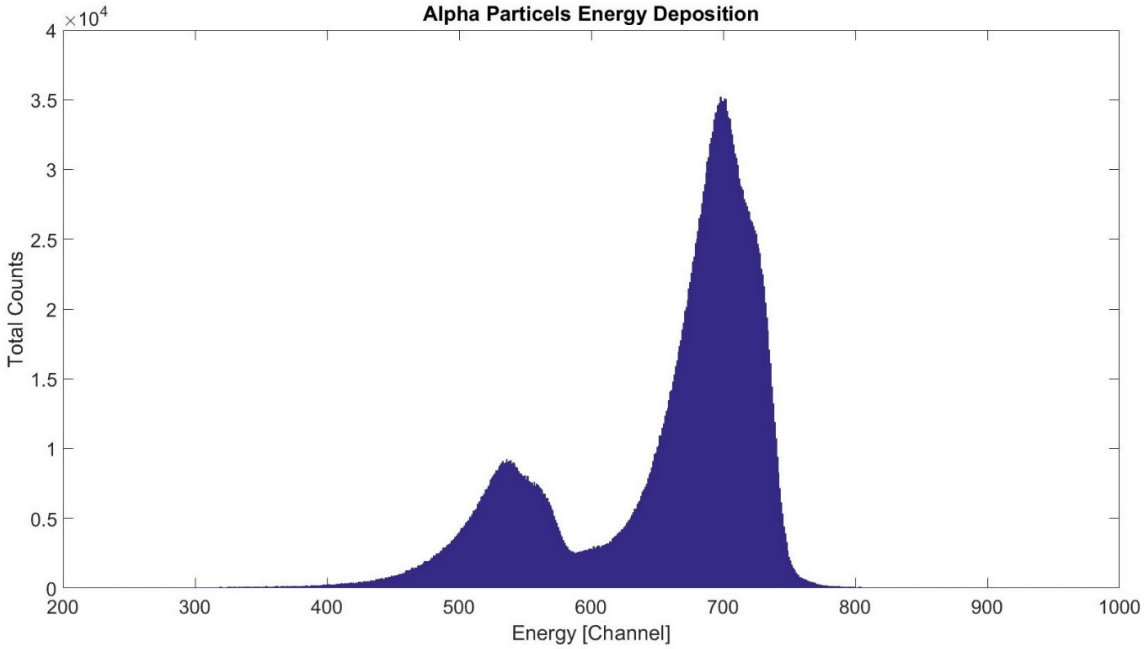

Figure 15. Energy deposition in the Millipore mixed cellulose filter by alpha particles from radon progeny. The peaks due to ^{218}Po and ^{214}Po are evident. 22.5 hours of measurement in Grenchen 1.

2019 JINST 14 P10019

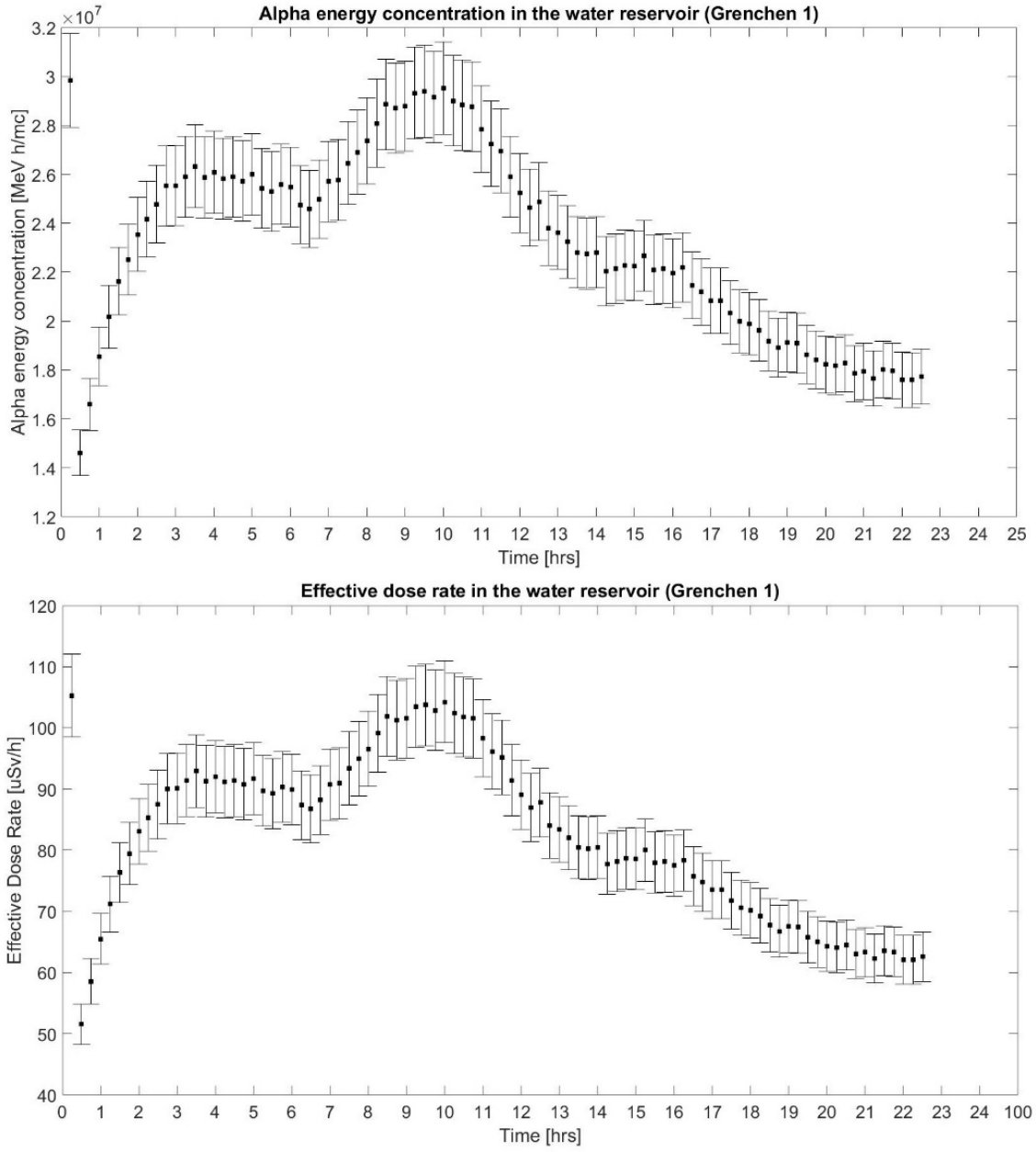

Figure 16. Alpha energy concentration and effective dose rate as a function of time in Grenchen 1.

radon and its progeny as a function of time. Figure 19 shows the radon concentration measured by the embedded ion chamber and the effective dose rate as a function of time. Although the time resolution of RaDoM2 is 15 minutes, the average value of the concentration and the effective dose rate are plotted integrated over two hours. The effective dose rate in Grenchen 2 in about 10 times lower than in Grenchen 1. The result is in good agreement with the different radon concentrations in the two water reservoirs. Figure 20 shows the effective dose rate estimated by the RaDoM2 (in red) and calculated by the radon concentration measured by the integrated ionization chamber (in black), assuming an equilibrium factor of 0.4 and a percentage of unattached radon daughters of 8%.

2019 JINST 14 P10019

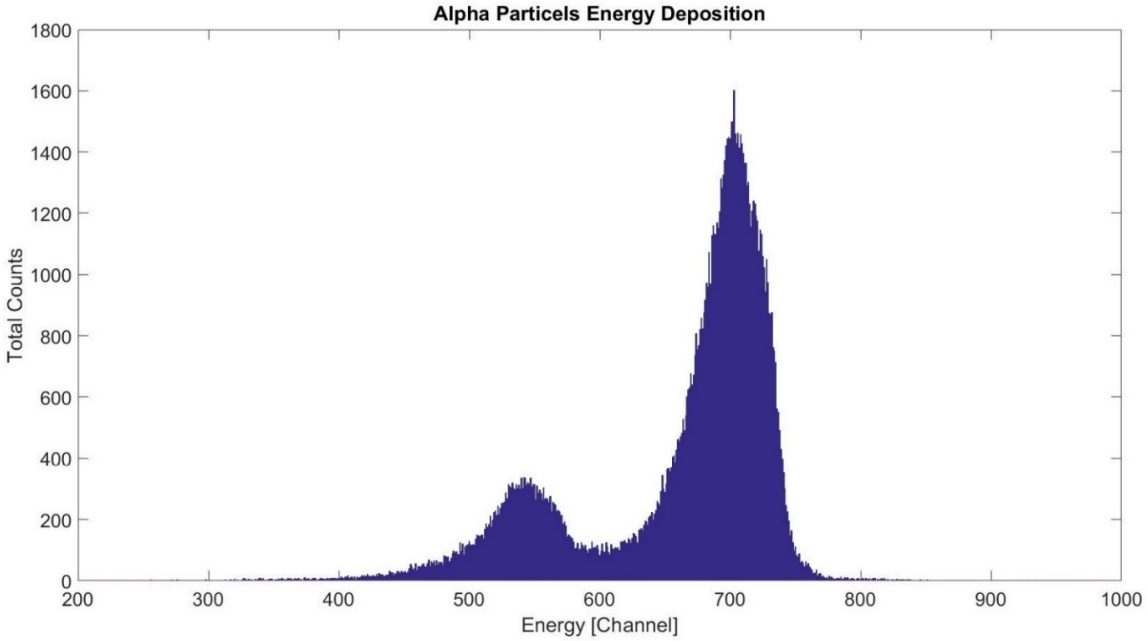

Figure 17. Energy deposition on the Millipore mixed cellulose filter by alpha particles from radon progeny. The peaks due to ^{218}Po and ^{214}Po are evident. 8.7 days of measurement in Grenchen 2.

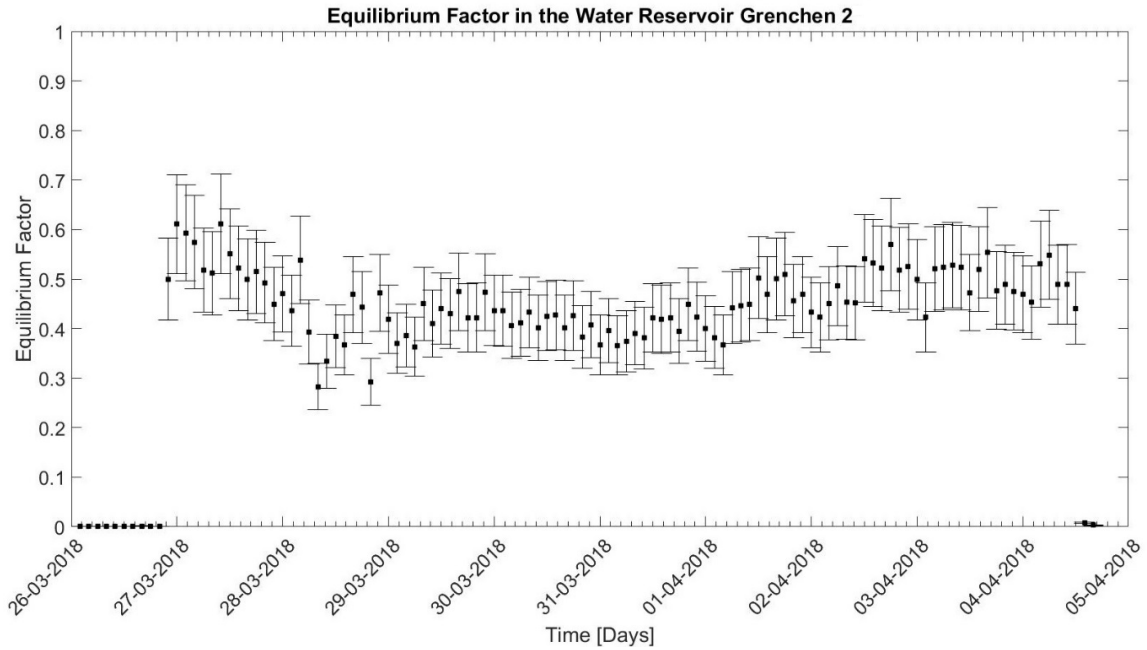

Figure 18. Time variation of the equilibrium factor in Grenchen 2.

2019 JINST 14 P10019

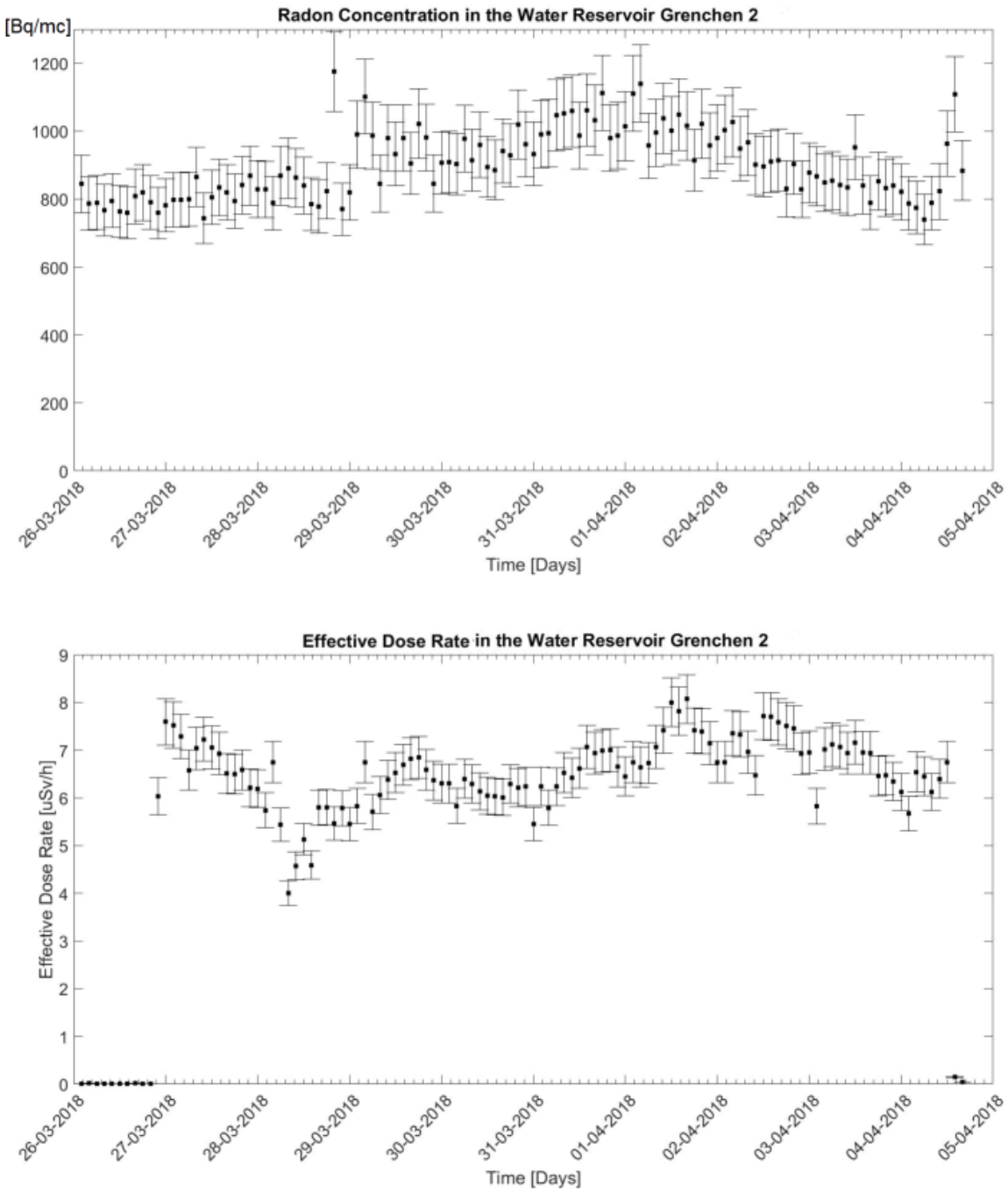

Figure 19. Radon concentration measured by the embedded ion chamber and effective dose rate as a function of time in Grenchen 2.

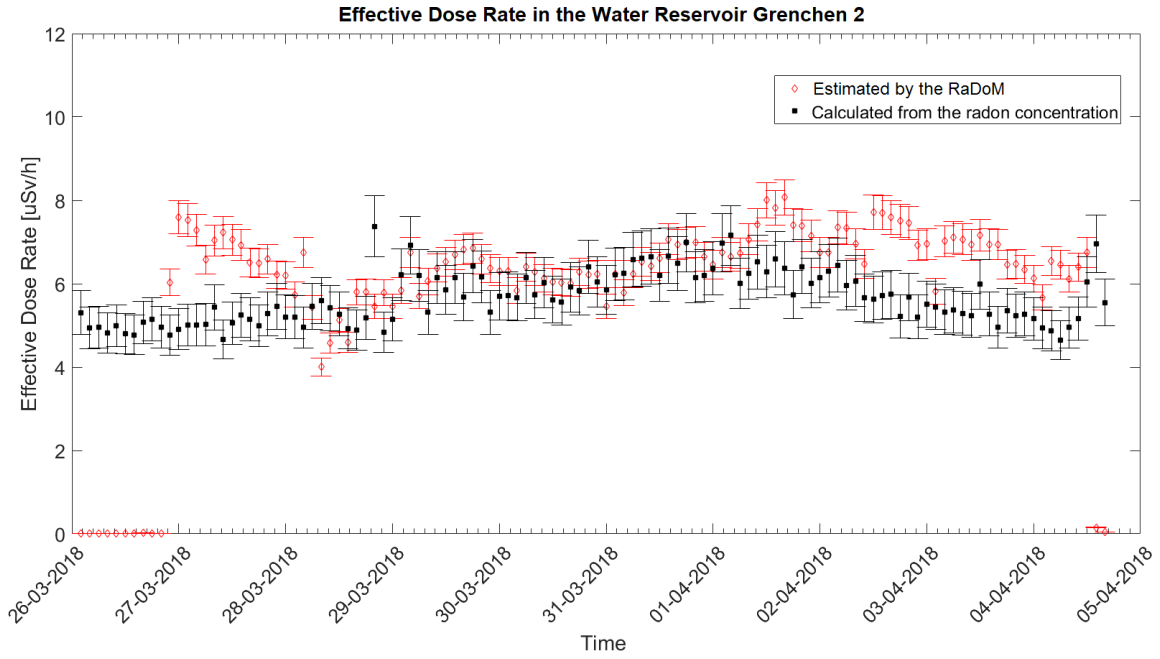

Figure 20. Effective dose rate as a function of time in Grenchen 2 calculated from the radon concentration (black) and estimated by the RaDoM2.

3.3 Discussion

A discussion on the uncertainties presented in the plots is needed. The response of RaDoM2 depends on various factors, such as the radon concentration, the quantity of airborne particles in the ambient air, their size and shape, etc. Such factors are influenced by the environmental conditions, by the presence (or not) of a ventilation system and in general by the number of air changes per hour. This is the correct behaviour for a detector designed to have a response that closely mimics the human lung, but also makes the estimation of the measurement uncertainties more complicated. A correct calibration is next to impossible in the CERN radon chamber as this is not a reference chamber. There is no information on the airborne particulate inside and it is difficult to maintain stable conditions over a long period of time: the radon, once is pumped in, starts to decay with its half life of 3.8 days. In addition, the RaDoM2 pumps and filters the air with a flow rate of 3 liters per minutes, effectively cleaning the chamber from radon in a few hours. Therefore considering only the statistical uncertainties is not sufficient, as can be seen from the plots of the measurements in Grenchen 1 and 2 (figures 16 and 19). The statistical uncertainties are in fact 0.6% and 1.8%, respectively. In order to estimate the overall uncertainties, the standard deviation was calculated during 12.5 hours of measurements in Grenchen 2, where both radon concentration measurements and dose measurements were stable. The hypotheses is that in an indoor environment without air exchange with stable temperature and humidity conditions, the quantity and quality of the airborne particulate is also stable, at least better than in the CERN radon chamber. Figure 21 shows the count distribution in the 12.5 hours dose measurement in Grenchen 2. Using this method the global uncertainty is 3.3%.

2019 JINST 14 P10019

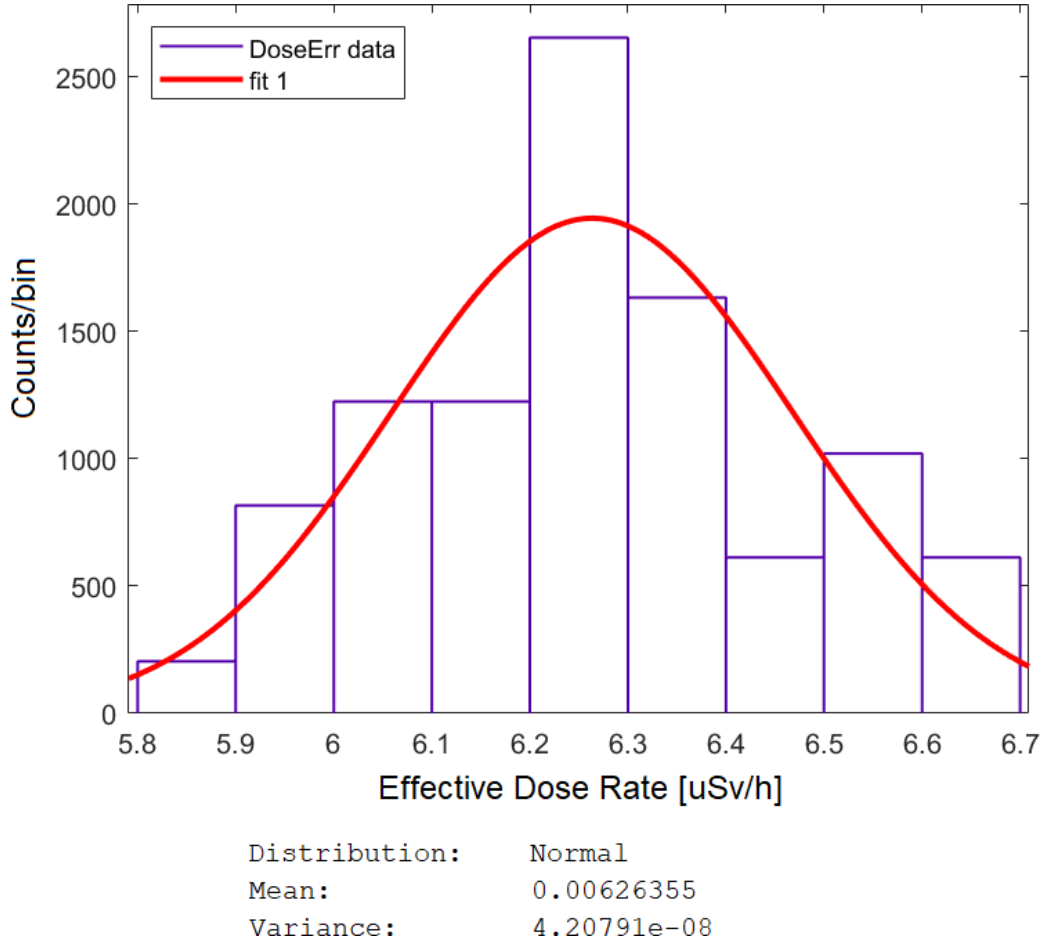

Figure 21. Count distribution during a 12.5 hour measurement in Grenchen 2. The statistical analysis was performed with data expressed in mSv/h

4 Conclusions

RaDoM2 shows improved performance as compared to RaDoM, mostly because of the improved pump flow and geometry. As with RaDoM, the results of the on-the-field measurements are consistent: the effective dose calculated from the radon concentration and directly estimated by RaDoM2 are comparable when the equilibrium factor is close to the standard value of 0.4, but RaDoM2 provides a much more accurate dose estimate when the conditions of the particulate in the air are far from the standard values, as inside the radon chamber. The response of RaDoM2 showed to be uncorrelated to the radon concentration and reasonably dependent on the activity concentration of the radon progeny, proving its capability to operate as a dosimeter. Furthermore, the integration of an ionization chamber in the board makes RaDoM2 a complete and powerful indoor monitoring station, able to measure the radon concentration, estimate the effective dose and calculate the equilibrium factor. Finally, thanks to the improved user interface and the cloud infrastructure, RaDoM2 is user-friendly, a particularly significant aspect if considering that radon monitors are radiation detectors of interest to the general public. CERN has recently licensed the RaDoM technology to the start-up company BAQ Sàrl (Switzerland) for developing a commercial version.

2019 JINST 14 P10019

Acknowledgments

This research was partly supported with funds from AIDA2020 Proof-of-Concept and CERN Medical Applications. We wish to thank Fabrizio Murtas (INFN, Italy) for his help and suggestions for the laboratory tests.

References

[1] S. Romano, M. Caresana, L. Garlati, F. Murtas and M. Silari, *RaDoM: a lung dosimeter for radon progeny*, 2018 *JINST* **13** P07030.

[2] X. Llopart, R. Ballabriga, M. Campbell, L. Tlustos and W. Wong, *Timepix, a 65k programmable pixel readout chip for arrival time, energy and/or photon counting measurements*, *Nucl. Instrum. Meth.* **A 581** (2007) 485 [*Erratum ibid.* **A 585** (2008) 106].

[3] Medipix website, http://medipix.web.cern.ch/medipix/.

[4] T.T.K. Cheung, K.N. Yu and D. Nikezic, *Bronchial dosimeter for radon progeny*, *Appl. Radiat. Isot.* **55** (2001) 707.

[5] Formlabs website, https://formlabs.com/store/.

[6] Autodesk Inventor website, https://www.autodesk.it/products/inventor/overview.

[7] I. Takeshi, F. Kenzo, T. Shinji and K. Ryuhei, *Characteristics of major filters used for ^{222}Rn progeny measurements*, *Radiat. Meas.* **29** (1998) 161.

[8] Comsol website, https://www.comsol.com/.

[9] https://www.cremat.com/CR-111-R2.1.pdf.

[10] https://www.cremat.com/CR-200-R2.1.pdf.

[11] http://radonftlab.com/.

[12] R. Tykca and J. Sabol, *Low level environmental radioactivity*, TECHNOMIC Publishing Co. Inc. (1995).

[13] ICRP 2017, *Occupational Intakes of Radionuclides: Part 3*, ICRP Publication 137, Ann. ICRP 46(3/4).

[14] https://www.nextome.net/.

[15] http://www.tecnavia.com/eedition/environment/.

[16] S. Bing, *CR-39 radon detector*, *Nucl. Tracks Radiat. Meas.* **22** (1993) 451.

2019 JINST 14 P10019